Journal of Material Sciences & Engineering

Commentary Open Access

Glycerol Carbonylation with CO_2 to Producing the Glycerol Carbonate over Metal Oxide Nanoparticle Catalyst and the Influence of Both the Calcination Temperature of the Catalyst and the Reaction Parameters

AL-Kurdhani JMH[1,3]*, Huajun Wang[1,2] and Elrasheed Elhaj[1]

[1]*Key Laboratory for Material Chemistry for Energy Conversion and Storage, Ministry of Education, School of Chemistry and Chemical Engineering, Huazhong University of Science and Technology, Wuhan 430074, PR China*

[2]*Hubei Key Laboratory of Material Chemistry and Service Failure, Huazhong University of Science and Technology, Wuhan 430074, PR China*

[3]*Industrial Research and Development Directory, Ministry of Sciences and Technology, Baghdad, Iraq*

Abstract

Four types of metal oxide nanoparticle catalysts (La_2O_3, NiO, CuO, and Co_3O_4) are prepared by precipitation method and used for the synthesis of glycerol carbonate from the direct carbonylation of glycerol and carbon dioxide in the presence of dehydrating agent and solvent. The effects of calcination temperatures, dehydrating agents, and reaction parameters on the conversion of glycerol and yield of glycerol carbonate are investigated. XRD, FT-IR, SEM, BET, CO_2-TPD, H_2-TPR and ICP-MS are used for the characterization of the prepared catalysts. It is found that the efficient catalyst for the carbonylation of glycerol should have not only large amount of basic sites and surface area, but also high redox ability and oxygen vacancy. CuO with calcination at 400°C exhibits higher catalytic activity and the best dehydrating agent is 2-Cyanopyridine. The active site of CuO catalyst may be crystal face (111). Under condition of 150°C, 4 MPa, 5 h, the glycerol carbonate yield can reach about 40%. The catalyst can be reused five times with little loss of activity and can be easily regenerated by calcination at 400°C.

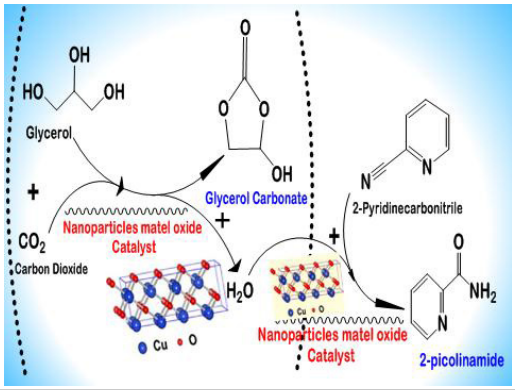

Keywords: Glycerol carbonate; Carbon dioxide; Metal oxide; Nanoparticle catalyst

Introduction

In recent decade, as a renewable and clean fuel, the biodiesel has attracted a great deal of interest in the whole world. It is predicted that the global production capacity of biodiesel will reach 50 million tons a year in 2020 [1-5]. In the industry, the biodiesel is mainly produced by the transesterification of animal or vegetable oil with methanol. In the process, glycerol (GL) is also rapidly produced as a main by-product at a rate of 10% of biodiesel production, resulting in a large surplus over traditional requirements in the chemical industry [6,7]. Therefore, more and more attention are drawn on transforming GL to high value-added products, such as acrolein, 1,3-propanediol, polyglycerols, and glycerol carbonate (GC). GC has many potential applications due to its low toxicity, high boiling point, and good biodegradability. It can be used as surfactant, adhesive, and paint as well as a component in gas separation membranes. GC also can serve as a useful solvent in lithium-ion batteries and a monomer for polymers such as polyesters, polycarbonates, polyurethanes, and polyamides [8-15].

GC can be synthesized from GL via several routes, which can be divided into two categories: indirect and direct routes, according to different carbonyl sources. GC can be indirectly synthesized by the transesterification of GL with other organic carbonates and urea. However, carbonates such as dimethyl or diethyl carbonate would be relatively expensive chemicals leading to less commercial benefit for the transesterification of GL with them [16-18]. Meanwhile, ammonia is produced in the glycerolysis of urea, which low-pressure reaction needs condition to remove the ammonia gas [19-22]. Compared with the indirect route, the direct synthesis of GC by GL carbonylation with CO_2 is more interesting and its atom utilization is as high as 87%

***Corresponding author:** Al-Kurdhani JMH, Key Laboratory for Material Chemistry for Energy Conversion and Storage, Ministry of Education, School of Chemistry and Chemical Engineering, Huazhong University of Science and Technology, Wuhan 430074, PR China, Tel: +86-13164696930; E-mail: jas_khay@yahoo.com

Received April 26, 2019; **Accepted** May 10, 2019; **Published** May 17, 2019

Citation: AL-Kurdhani JMH, Wang H, Elhaj E (2019) Glycerol Carbonylation with CO_2 to Producing the Glycerol Carbonate over Metal Oxide Nanoparticle Catalyst and the Influence of Both the Calcination Temperature of the Catalyst and the Reaction Parameters. J Material Sci Eng 8: 523.

[23,24]. Moreover, this reaction is regarded as a green process in which two cheap raw reactants, GL, a by-product of biodiesel production, and CO_2, a primary greenhouse gas, can be converted to a value-added chemical, GC.

Up to now, a series of catalysts were used to catalyze the carbonylation of GL with CO_2, such as basic ion-exchange resin, CeO_2-Al_2O_3 or CeO_2-Nb_2O_5, tin complexes, Cu/La_2O_3, $La_2O_2CO_3$/ZnO and so on [25-28]. However, a low GL conversion was obtained over these catalysts because of thermodynamic limitation. Vieville et al. used GL and supercritical carbon dioxide as reactants by using basic ion-exchange resin as a catalyst to obtain GC, but the reaction did not occur [25] Aresta et al. employed CeO_2-Al_2O_3 and CeO_2-Nb_2O_5 as catalyst using tetra (ethylene glycol) dimethyl ether as the solvent, and the conversion of GL only reach 2.5% after 15 h reaction [24]. Recently, in order to overcome the thermodynamic limitation, some agents, such as acetonitrile and 2-Cyanopyridine, were used as dehydrant in the carbonylation of GL with CO_2 and a little enhanced GL conversion was obtained [27]. Despite of these progresses, the conversion of GL is still relatively low and it is a challenge to develop new effective catalytic system.

Metal oxide nanoparticle is an important kind of catalysts with a high surface area and a high catalyst activity. In more and more reactions, metal oxide nanoparticle works as a catalyst showing very good performance [29-31]. For instance, Paulose et al. prepared nano copper oxide (CuO) dispersed on alumina by sol-gel method and found the catalyst shows high catalytic activity for the thermal decomposition of ammonium perchlorate [31]. Shokrani et al. [32] also synthesized CuO-based nanocatalyst by urea-nitrates combustion method and found that the nanocatalyst has a well practicability for hydrogen production via steam reforming of methanol In present work, four types of metal oxide nanoparticle catalysts (La_2O_3, NiO, CuO, and Co_3O_4) were prepared by precipitation (TP) method and used for the synthesis of GC from the direct reaction of GL and CO_2 with the dehydrating agent (such as 2-Cyanopyridine) and solvent (such as DMF). XRD, FT-IR, SEM, BET, CO_2-TPD, H_2-TPR and ICP-MS were used for the characterization of the prepared metal oxide catalysts. It is found that the best metal oxide nanoparticle catalyst is CuO. The effects of calcination temperature, type of dehydrating agents, and reaction parameters on the GL conversion and GC yield were researched in detail. To the best of our knowledge, the present work is the first one about the using CuO nanoparticle as catalyst in the reaction of GL with CO_2 to produce GC.

Experimental Section

Chemicals

Copper nitrate [$(Cu(NO_3)_2.3H_2O$] (99% purity), lanthanum nitrate [$La(NO_3)_3.6H_2O$] (98% purity), nickel nitrate [$(Ni(NO_3)_2.6H_2O$] (98% purity), ammonia solution (25 wt.%), GL (99% purity), methanol (99.5% purity), acetonitrile (99% purity) and N.N-dimethyl formamide (DMF) (C_3H_7NO) (99.5% purity) were purchased from Sinopharm Chemical Reagent Co., Ltd., Beijing, China. 4-Cyanopyridine (98% purity), 2-Cyanopyridine (2-Pyridinecarbonitrate ($C_6H_4N_2$) (98% purity), cobalt acetate [$Co(CH_3COO)_2.4H_2O$] (99.9% purity), tetra ethylene glycol (99% purity), and 2-Picolinamide (>98% purity) were purchased from Aladdin Industrial Corporation, Shanghai, China. Carbon dioxide (99.9% purity) was supplied by Wuhan Minghui Gas Technology Co., Ltd., Wuhan, China. GC (Tokyo Chemical Industry Co., Ltd., Tokyo, Japan) was of over 90% purity. All these chemicals were used without further purification.

Catalyst preparation

Metal oxide nanoparticle catalysts, La_2O_3, NiO, CuO, and Co_3O_4, were prepared by the precipitation (PT) method. CuO is used as the example to introduce the method. 7.55 g of copper nitrate ($Cu(NO_3)_2.3H_2O$) was firstly dissolved in 250 mL of deionized water in a 500 mL round bottom 3-neck glass flask (the molar concentration for copper nitrate was 0.125 mol/L), then, the solution was heated to 80°C by using oil bath and held about 1 h with vigorous stirring. After an appropriate amount of ammonia solution (1.0 mol/L) was added into the mixture, keeping the pH value (10 ± 1), a nanoparticle suspension was formed quickly. The precursor was aged at 60°C for 1 h, filtered and washed with deionized water for five times, and after that dried at 60°C in vacuum dryer for 2 h, and then grinded to 100 mesh scale, followed by calcination at 400°C for 5 h in air. The obtained product was denoted as CuO-PT-400. Other metal oxide nanoparticle catalysts were also prepared by the same procedure using corresponding salt. The samples calcined at different temperatures were named as M_xO_y-PT-T (T means the calcination temperature).

Catalyst characterization

X-ray diffraction (XRD) patterns of the catalysts were measured on a X'Pert PRO using Cu Kα radiation at 30 kV and 15 mA, over a 2θ range of 5-90° with a step size of 0.0167° at a scanning speed of 8 min^{-1}. A Bruker VERTEX 70 FT-IR spectrometer was used to obtain the FT-IR spectra of samples using KBr pellet technique, with 2 cm^{-1} resolution over the wavenumber range 4000-400 cm^{-1}.The morphology of the particles was observed by use of a scanning electron microscope (SEM, TESCAN VEGA3) with 20.0 kV of an accelerating voltage.

Nitrogen adsorption-desorption isotherms were determined by a volumetric adsorption apparatus (Micromeritics ASAP 2420) at 77 K. The surface areas of samples were calculated by using the Brunauer-Emmett-Teller (BET) method. The pore volume was given at p/p_0=0.99. The pore size distribution was calculated by the Barrett-Joyner-Halenda (BJH) method.

Also, the basicity studies of the prepared catalysts were conducted with temperature-programmed desorption of CO_2 as probe molecule (CO_2-TPD) using Huasi DAS-7000 apparatus equipped with thermal conductivity detector (TCD). The analysis was performed by heating 100 mg of the catalyst sample under a (He) flow from room temperature to 800°C for 2 h (10°C/min, 50 mL/min). Then, the temperature was decreased to 90°C, and a flow of pure CO_2 (50 mL/min) was subsequently introduced into the reactor during 1 h. After the catalyst was swept with (He) for 1 h to remove the physically adsorbed CO_2 from catalyst surface, the TPD of CO_2 was carried out between 90°C and 900°C under a (He) flow (10°C/min, 30 mL/min) and the detection of the desorbed CO_2 was by an on-line gas chromatograph provided with a TCD.

H_2 temperature programmed reduction (H_2-TPR) measurements were carried out on the CHEMBET 3000 TPR/TPD instrument. Before the reduction, a sample was preheated in Ar gas (30 mL/min) at 400°C for 30 min to remove surface contaminants. After the sample cooled down to 50°C, a mixture of 5.01% H_2/Ar was flowing through the reactor and the temperature was increased from 30°C to 920°C. The hydrogen consumption was monitored by a TCD detector.

Inductively coupled plasma-mass spectrometry (ICP-MS) is a powerful tool for analyzing trace metals in environmental samples. A large range of elements can be detected using an (ICP-MS) ELAN DRC-e Axial Field Technology. Lab Method 3050:1T was the acid digestion method to prepare the sample for (ICP-MS) analysis.

Reaction procedure

Glycerol carbonate (GC) was obtained from the carbonylation of glycerol (GL) and CO_2 over nanoparticles metal oxide catalysts. As shown in Scheme 1.

The tests of the catalytic activities of the nanoparticles metal oxide catalysts were carried out in a stainless-steel autoclave reactor system with an inner volume of 200 ml and it has thermostat with an electric heating jacket, pressure gauge and agitator, the autoclave reactor was one of the most important chemical engineering equipment and its operation is not easy, it requires attention and caution when operating, because it works under conditions of high temperature and high pressure. After ascertaining the validity of the autoclave system (Figure 1), the typical procedure is as follows: 40 mmol glycerol (GL), 37 mmol% Cat./GL, 16 g of Dimethylformamide (DMF) and 6 g of 2-Pyridinecarbonitrate , were added into the autoclave together, and then the reactor was sealed, purged with N_2 or CO_2 for 3 times and then pressurized with CO_2 to 4 MPa. Subsequently, the autoclave was heated to the reaction temperature (150°C) and maintained for certain reaction time (5 h) under vigorous stirring. After reaction, the reactor was cooled to room temperature and depressurized, the product mixture was taken out from the autoclave reactor to centrifugal filtration 5000 rpm for 6 min to separation the solid catalyst and liquid products, after that take all liquid product to analyzing.

Liquid product analysis

All the components of liquid product were analyzed by the gas chromatograph (Fuli 9790-II) equipped with a flame ionization detector (FID) and a capillary column KB-WAX (30 m long, 0.25 mm i.d.). The internal standard method was used. Tetraethylene glycol was used as an internal standard to determine GL and GC. Nitrogen (99.999 %, Sichuan Tianyi Science and Technology Co., Ltd., Sichuan, China) was used as the carrier gas with a flow rate of 30 mL/min at 0.3 MPa. The temperatures of the injector and the detector are 250°C and 270°C, respectively. The temperature of the column was programmed to have a 2-min initial hold at 70°C, a 15°C/min ramp from 70°C to 250°C and then a 15 min hold at 250°C. A good peak separation was achieved under these conditions for all components. Added about 1 g methanol to liquid product sample for diluting and added internal standard n-Butanol and tetra ethylene glycol for determine Methanol and both (GL and GC) respectively before injecting into gas chromatograph (Fuli 9790-II) for determining the mass and mole of GL and GC output with product.

The conversion of GL, X_{GL}, the yield of GC, Y_{GC}, and the selectivity to GC, S_{GC} were calculated according to the following equations:

$$X_{GL} = \frac{n_{GL}^{in} - n_{GL}^{out}}{n_{GL}^{in}} \times 100\% \quad (1)$$

$$Y_{GC} = \frac{n_{GC}^{out}}{n_{GL}^{in}} \times 100\% \quad (2)$$

$$S_{GC} = \frac{n_{GC}^{out}}{n_{GL}^{in} - n_{GL}^{out}} \times 100\% \quad (3)$$

Where n_{GL}^{in} the initial mole number (mol.) of GL, while n_{GL}^{out} and n_{GC}^{out} are the mole numbers (mol) of GL and GC in the residual reaction mixture after reaction, respectively.

Results and Discussion

Effect of type of metal oxide nanoparticle catalyst

In this work, the GC is produced from the direct carbonylation of GL and CO_2 over metal oxide nanoparticle catalyst (such as CuO) with the hydrolysis of dehydrating agent (such as 2-Cyanopyridine) as the coupling reaction. As shown in Scheme 2, all the reaction process contains two steps: firstly, GL reacts with CO_2 to produce GC and the byproduct was water, and then secondly the formed water is removed from the middle of reaction by reacting with the 2-Cyanopyridine to produc 2-Picolinamide. The gas chromatogram of the reaction mixture

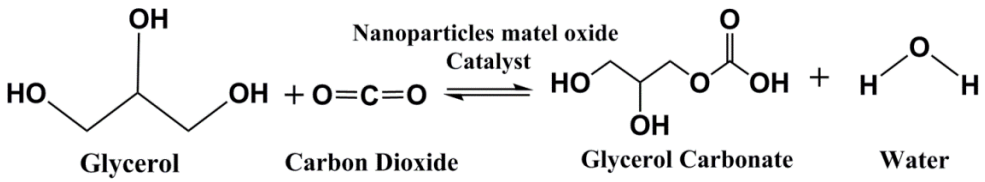

Scheme 1: Reaction of glycerol and CO_2 (carbonylation of glycerol) over nanoparticles metal oxide catalysts.

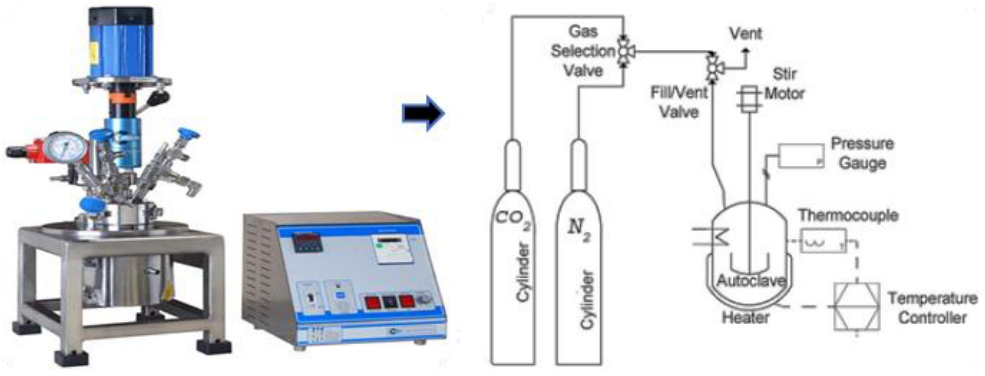

Figure 1: Autoclave reactor system.

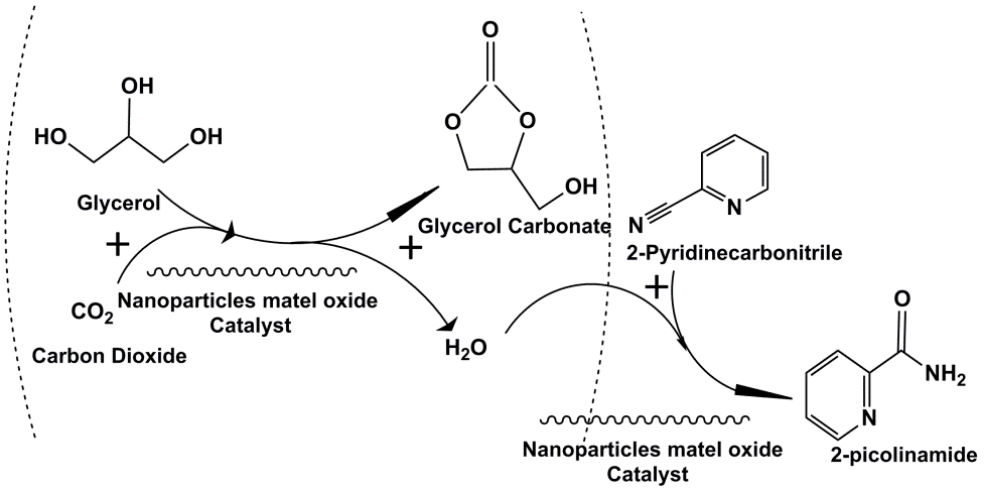

Scheme 2: Pathway of carboxylation of glycerol (GL) and hydration of 2-Cyanopyridine over nanoparticle metal oxide catalysts.

is given in Figure 2. It can be found a good peak separation is achieved for all components.

Four types of metal oxide nanoparticle catalysts, CuO-PT-400, Co_3O_4-PT-400, La_2O_3-PT-400, and NiO-PT-400 were prepared by PT method and used in carbonylation of GL with CO_2 to produce GC and their catalytic performances were presented in Table 1. Among these catalysts, the CuO-PT-400 nanoparticle has the highest catalytic performance; in contrast, NiO-PT-400 shows the lowest activity for the reaction of GL with CO_2. Over CuO-PT-400 catalyst, the GL conversion, GD yield, and GD selectivity can reach 48.64%, 38.88%, and 79.94%, respectively. The results mean CuO-PT-400 nanoparticle is a good catalyst for carbonylation of GL with CO_2.

Effect of the calcination temperature

In general, the particle size has an important effect on the activity of metal oxide nanoparticle catalyst. By means of varying the calcinations temperature, the crystallite size and catalytic activity of CuO nanoparticle can be manipulated. In order to scrutinize the effect of calcination temperature on the catalyst activity, several CuO nanoparticles were prepared by calcination at 300°C, 400°C, and 500°C, respectively, and examined in the carbonylation of GL with CO_2. It can be seen from Table 1, as the calcination temperature increases from 300°C to 400°C, the GL conversion slightly increases form 45.39% to 48.64% while the GC yield and GC selectivity, however, remarkably increase from 17.72% and 39.03% to 38.88% and 79.94%, respectively. When the calcination temperature further increases to 500°C, the GL conversion decreases to 32.58%, meanwhile, the GC yield and GC selectivity strikingly decrease to 7.72% and 23.70%. It indicates that the calcination temperature has a significant effect on the catalytic activity of the CuO nanoparticle. So, 400°C is a suitable calcination temperature for the CuO nanoparticle catalyst.

Effect of dehydration agents

Because the direct carbonylation of GL with CO_2 is limited seriously by thermodynamics, the dehydrating agents are necessary to shift the chemical equilibrium to the GC production side. The effect of several dehydration agents including 4-cyanopyridine, acetonitrile, and 2-Cyanopyridine are researched and the results are given in Figure 3. It shows that when there is not any dehydration agent for the reaction

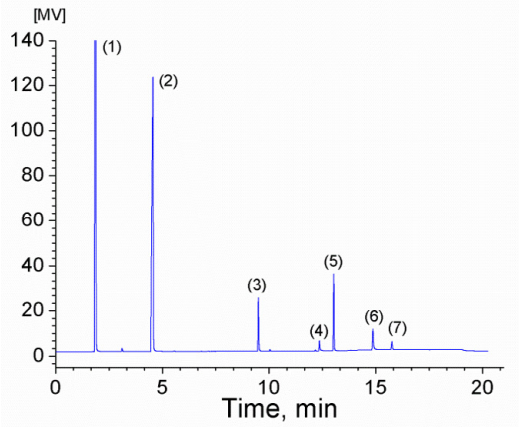

Figure 2: The gas chromatogram of the reaction mixture (1) methanol, (2) DMF, (3) 2-Cyanopyridine, (4) GL, (5) 2-Picolinamide, (6) tetraethylene glycol, (7) GC.

Cat.	X_{GL}/%	Y_{GC}/%	S_{GC}/%
CuO-PT-400	48.64	38.88	79.94
Co_3O_4-PT-400	20.58	7.77	37.78
La_2O_3-PT-400	22.62	12.14	53.65
NiO-PT-400	34.01	6.21	18.26
CuO-PT-300	45.39	17.72	39.03
CuO-PT-500	32.58	7.72	23.70

[a]Reaction condition: 40 mmol GL, 5 g of 2-Cyanopyridine,1.2 g catalyst, 15 g DMF, 150°C, 4 MPa CO_2, 5 h

Table 1: The catalytic performances of the metal oxide nanoparticle catalysts in the carbonylation of GL with CO_2 to produce GC [a].

of GL with CO_2, the GL conversion and GC yield only reach 22.76% and 1.52%, respectively. On the contrary, the dehydration agent, especially 2-Cyanopyridine, can remarkably increase the catalytic activity. When 2-Cyanopyridine is used as dehydration agent, the GL conversion and GC yield can respectively reach 48.64% and 38.88%, while for 4-cyanopyridine as dehydration agent, the GL conversion and GC yield reach 43.0% and 28.16%. However, acetonitrile is not a good alternative for the GL conversion and GC yield only reach 14.07% and 2.19%, respectively, by using acetonitrile as dehydration agent. It means that 2-Cyanopyridine is a good dehydration agent for the carbonylation of GL with CO_2.

Catalyst characterization

XRD: Figure 3 shows the XRD patterns of CuO nanoparticle catalysts calcined at different temperature (300°C, 400°C, and 500°C). All the samples present a typical band of CuO phase with monoclinic crystal system (at 2θ=32.5, 35.5, 38.8, 46.2, 48.8, 51.4, 53.5, 58.3, 61.5, 66.3, 68.13, 72.5, 75.1, 80.1, 82.5, 83.1, 83.6, see PDF 01-089-5898), indicating that the calcination temperature has no remarkable effect on the crystal structure of CuO nanoparticle. In Figure 4, it is also found that for CuO-PT-400 sample at 2θ=38.709 and *I*=99.0%, the diffraction intensity of crystal face (111) is stronger than of crystal face (110) at 2θ=32.509 and *I*=13.0%, in contrast, for CuO-PT-300 and CuO-PT-500, the diffraction intensity of crystal face (110) is stronger than of crystal face (111). It means that the calcination temperature has an effect on the growth and relative content of crystal face for CuO nanoparticle. Meanwhile, it is showed that the intensity of crystal face (111) increases in the following order for these samples: CuO-PT-400>CuO-PT-500>CuO-PT-300, which is accordant with the order of the catalytic activity for these catalysts (Table 1, except CuO-PT-500), meaning that crystal face (111) may be the active site for the carbonylation of GL with CO_2.

FT-IR: The FT-IR analysis results are depicted in Figure 5 for CuO nanoparticles with different calcination temperature. For all samples the peak positions are approximately similar indicating they have the same surface functional groups. The peaks appearing at 517 and 598 cm^{-1} are attributed to Cu-O stretching modes [32,33]. The peak at 1384 cm^{-1} may be assigned to O-H bending vibrations combined with copper atoms, which fade gradually when the calcination temperature is increased from 300°C to 500°C. Furthermore, peaks at around 3460 cm^{-1} show the existence of the hydroxide group. The FT-IR result suggests the formation of CuO compound and is consistent with the XRD.

SEM: The SEM images of the CuO nanoparticle catalysts are shown in Figure 6. It is found that all samples present aggregates of variable morphology and size. Both CuO-PT-300 and CuO-PT-500 have particles with two kinds of shapes: rodlike and nubbly and their particle size is about 1 μm, while CuO-PT-400 has spherical particles with about 300 nm. It means, among these samples, CuO-PT-400 has the particle with the smallest size and the most uniform shape, resulting in the best catalytic activity.

BET: The N_2 adsorption-desorption isotherms of the CuO

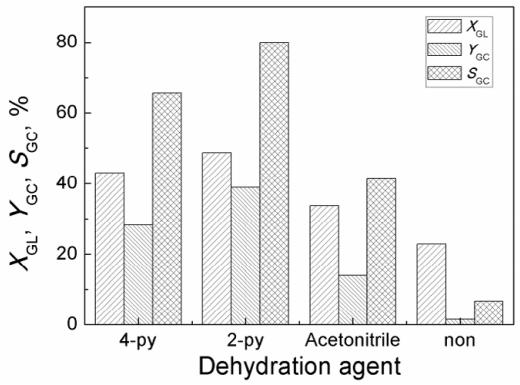

Figure 3: The effects of dehydration agents on carbonylation of GL with CO_2 to produce GC (Reaction condition: 40 mmol GL, 1.2 gcatalyst, 5 g of 2-Cyanopyridine, or 4-cyanopyridine, or acetonitrile, 15 g DMF (or 20 g when any dehydration agent is not used), 150°C, 4 MPa CO_2, and 5 h).

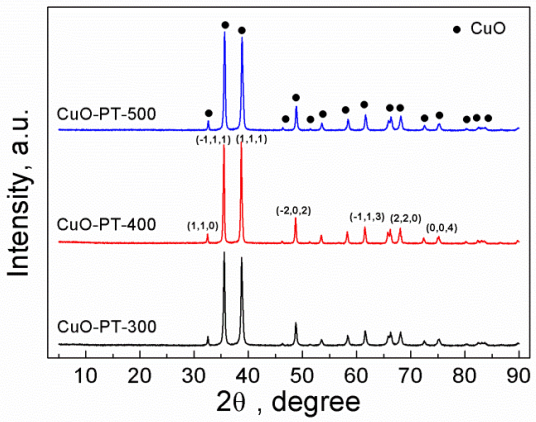

Figure 4: XRD patterns of the CuO nanoparticle catalysts calcined at different temperature: 300°C, 400°C, and 500°C.

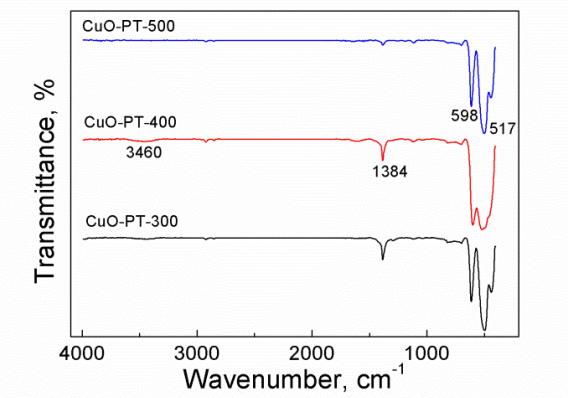

Figure 5: FT-IR spectra of CuO nanoparticles catalysts calcined at different temperature: 300°C, 400°C, and 500°C.

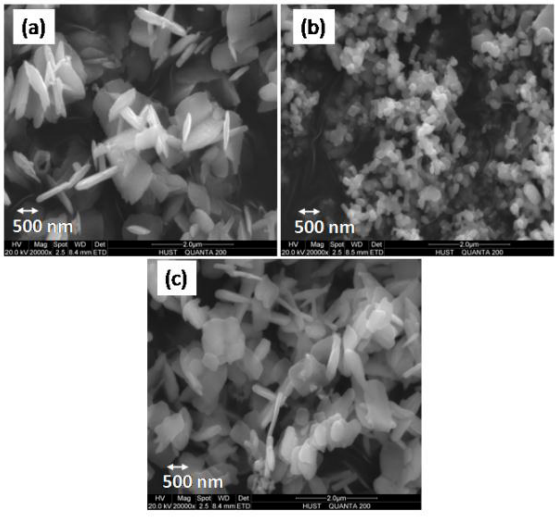

Figure 6: SEM images of the CuO nanoparticle catalysts (a) CuO-PT-300, (b) CuO-PT-400, and (c) CuO-PT-500.

nanoparticle catalysts calcined at different temperatures are presented in Figure 7. The related BET specific surface areas, total pore volumes, and average pore diameters are listed in Table 2. Two catalysts exhibited type IV isotherms with different shaped hysteresis loops in terms of the IUPAC classification. It is also found that the adsorbed quantity of CuO-PT-400 is larger than that of CuO-PT-500 meaning the specific area of CuO-PT-400 is higher. Table 2 shows that compared with CuO-PT-500, the CuO-PT-400 not only has higher BET surface area, but also bigger pore volume and pore diameter. It indicates that calcination at high temperature tends to result in agglomeration of the catalyst particles to reduce the surface area and pore volume. Obviously, the CuO-PT-400 is more suitable for the reaction of GL with CO_2 and obtained a higher GL conversion.

CO_2-TPD: The basicity of CuO nanoparticle catalysts is characterized by CO_2-TPD and the profiles are shown in Figure 8. In the TPD profiles of these samples, the peaks at the temperature range of 35~200°C, 200~380°C, and >380°C are attributed to desorption of CO_2 from weak, medium, and strong basic sites, respectively. By integrating these peak areas, the amounts of basic sites can be evaluated and the results are presented in Table 3. It shows that except the medium basic sites, the amounts of weak and strong basic sites increase with the increase of calcination temperature and the total amounts of the basic sites as well as. The results mean that the quantitative distribution of different strength basic sites and total amount of desorbed CO_2 are dramatically influenced by the calcination temperature. In general, a more basicity is beneficial for the carbonylation of GL with CO_2. Compared with CuO-PT-300, CuO-PT-400 has higher amount of basic sites, so it also has higher GC yield. It is also observed that among these samples, though CuO-PT-500 has the highest basicity, the GC yield on this sample is the lowest. The reason may be that CuO-PT-500 has lesser surface area and pore volume by the agglomeration of catalyst particles at high temperature, resulting in its lower catalytic activity.

H_2-TPR: The H_2-TPR was used to determine the redox ability and oxygen vacancy density of CuO nanoparticle catalysts. The H_2-TPR profiles of CuO are shown in Figure 9 and the data of H_2 consumption below 400°C are listed in the sixth column in Table 3. It is found that all of the samples have only one strong and sharp reduction peak, indicating that there may be a type of CuO species in these samples. Meanwhile, in these H_2-TPR profiles, the temperature of H_2 consumption maximum is different and they are 327°C, 277°C, and 332°C for CuO-PT-300, CuO-PT-400, and CuO-PT-500, respectively. In these samples, CuO-PT-400 has the lowest reduction temperature, meaning this sample can be easily reduced. In contrast, CuO-PT-500 has the highest reduction temperature, meaning this sample is reduced difficultly. These differences may be due to the difference of the particle size, surface area and morphology with various exposed crystal planes. The H_2 consumption can be a glancing representative of oxygen vacancy density and decreases with the increase of the calcination temperature (see the sixth column in Table 3), suggesting that CuO-PT-300 may have the highest oxygen storage/release capacity and CuO-PT-500 has the lowest. In the present work, we have found that the catalytic activity of CuO nanoparticle catalyst is connected to not only its amount of basic sites and surface area (see the discussion in 3.4.3~3.4.5 section), but also the redox ability and oxygen vacancy density. CuO-PT-400 with the best redox ability and a higher oxygen vacancy gives the

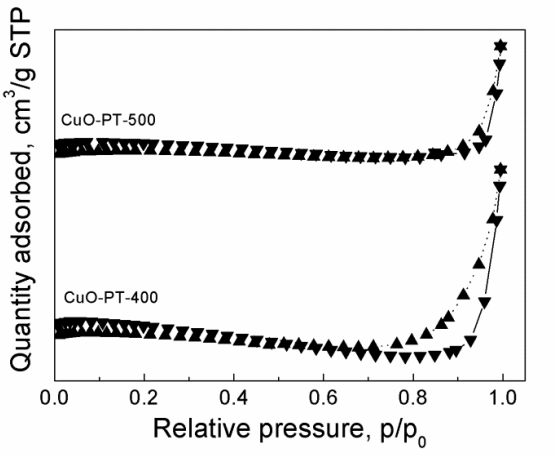

Figure 7: N_2 adsorption-desorption isotherms of the CuO nanoparticle catalysts calcined at different temperature: 400°C, and 500°C.

	S_{BET} (m^2/g)	Volume (cm^3/g)	Average pore diameter (nm)
CuO-PT-400	3.24	0.0168	20.71
CuO-PT-500	2.50	0.0107	17.12

Table 2: The BET surface area, pore volume, and pore diameter for the CuO nanoparticle catalysts. Total pore.

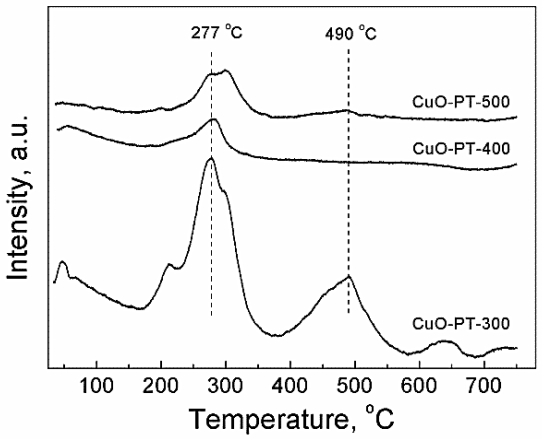

Figure 8: CO_2-TPD profiles of the CuO nanoparticle catalysts calcined at different temperature: 300°C, 400°C, and 500°C.

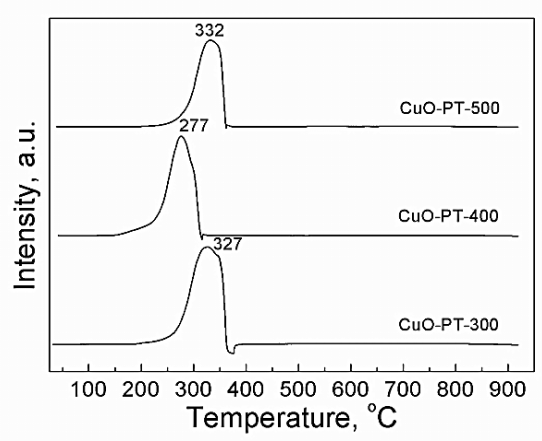

Figure 9: H_2-TPR profiles of the CuO nanoparticle catalysts calcined at different temperature: 300°C, 400°C, and 500°C.

highest yield of GC. In contrast, CuO-PT-500 produces the lowest GC yield because of the least oxygen vacancy and the weakest redox ability. Meanwhile, CuO-PT-300 with a medium redox ability and higher oxygen vacancy gives a medium GC yield, which is higher than CuO-PT-500 and lower than CuO-PT-400. On the basis of these understanding, it is not unreasonable to predict that the best catalyst for the synthesis of GC from carbonylation of GL with CO_2 should have not only high amount of basic sites and surface area, but also high redox ability and oxygen vacancy.

Effect of reaction conditions

Figure 10a shows the effect of reaction time on the catalytic activity of the CuO-PT-400 nanoparticle. As the reaction time increases to 5 h, the GL conversion, GC yield, and GC selectivity almost linearly increase to 48.64%, 38.88%, and 79.94%, respectively. However, when the reaction time further increases, the GC yield hardly changes. So, the suitable reaction time is 5 h.

The CO_2 pressure also has an important effect on the catalytic activity of CuO-PT-400. As shown in Figure 10b, as CO_2 pressure increases from 1.0 MPa to 2.0 MPa, the GL conversion only increases small and GC yield hardly changes. When CO_2 pressure further increases from 2.0 MPa to 4.0 MPa, both the GL conversion and GC yield rapidly increase to 48.64% and 38.88%, respectively. Meanwhile, the GC selectivity also remarkably increases to 79.94% with the increase of CO_2 pressure to 4.0 MPa. When the CO_2 pressure further increases, the GC yield slightly decreases. Thereby, 4.0 MPa of CO_2 pressure is optimized for the reaction of GL with CO_2.

Figure 10c presents the effect of reaction temperature on the catalytic activity of CuO-PT-400 nanoparticle. With the rise of reaction temperature from 100°C to 150°C, both the GL conversion and GC yield increase from 14.16% and 0.93 % to 48.64% and 38.88% as well as GC selectivity from 6.56% to 79.94%. With the further increase of the reaction temperature to over 150°C, the GC yield decreases. So, 150°C should be the suitable reaction temperature.

Figure 10d shows the weight of catalyst on the catalytic activity of CuO-PT-400. With the increase of weight of catalyst from 0.1 g to 1.2 g, both the GL conversion and GC yield increase rapidly from 35.08% and 8.97% to 46.0% and 28.68% at weight of catalyst of 0.3 firstly and then slowly increase to 48.64% and 38.88%, respectively. Meanwhile, the GC selectivity also increases from 24.72% to 79.94% with the rise of weight of catalyst. So, the suitable weight of catalyst is 1.2 g.

Stability of the CuO nanoparticle catalyst

The stability of CuO-PT-400 was also researched and the result is shown in Figure 11. It is found that at the fourth recycling, the activity of CuO-PT-400 hardly decreases and the GL conversion and GC yield

Cat.	CO_2 adsorption amount (μmol/g)				H_2 consumption (mmol/g)
	<200°C	200~380°C	>380°C	Total amount	
CuO-PT-300	9.67(20.9%)[a]	20.41(44.1%)	16.22(35.0%)	46.3	1.95
CuO-PT-400	13.80(27.3%)	15.00(29.7%)	21.70(43.0%)	50.49	1.66
CuO-PT-500	17.17(25.1%)	20.28(29.7%)	30.84(45.2%)	68.29	1.45

[a]the number in bracket is the percentage of different strength basic sites on total CO_2 desorption amount.

Table 3: The amount of CO_2 adsorption and H_2 consumption of CuO nanoparticle catalysts measured respectively by CO_2-TPD and H_2-TPR.

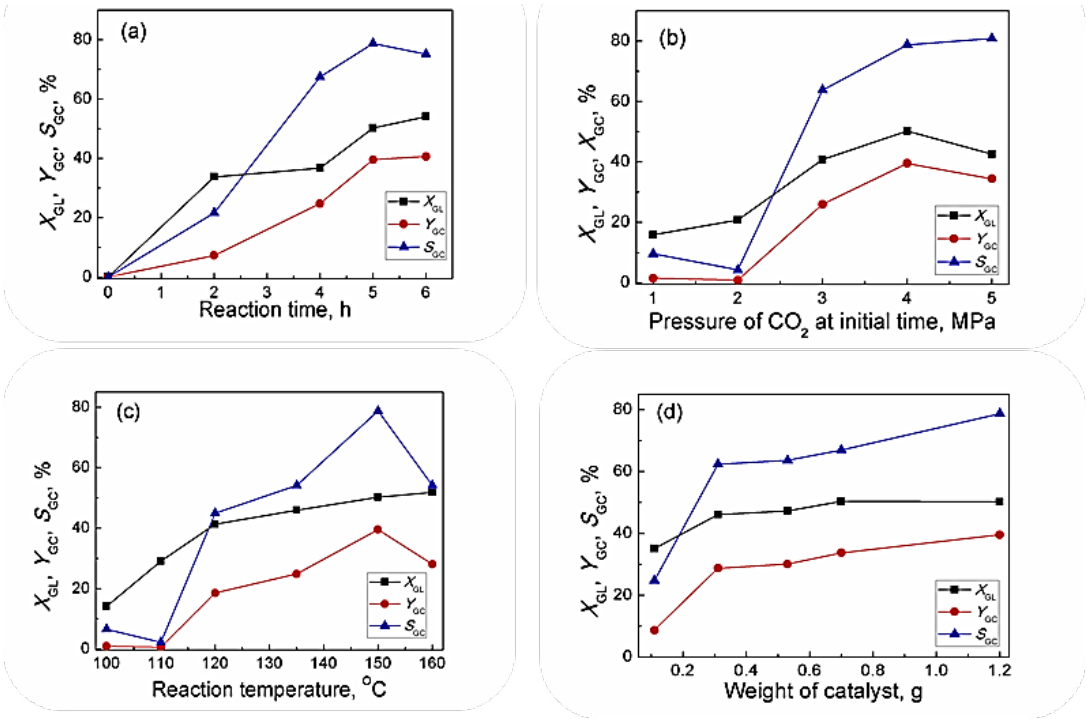

Figure 10: Effect of (a) reaction time, (b) pressure of CO_2, (c) reaction temperature, and (d) weight of catalyst on carbonylation of GL with CO_2 over CuO-PT-400 catalyst (Reaction condition: 40 mmol GL, 1.2 g Catalyst, 5 g of 2-Cyanopyridine, 15 g of DMF, 150°C, 4 MPa CO_2 and 5.0 h).

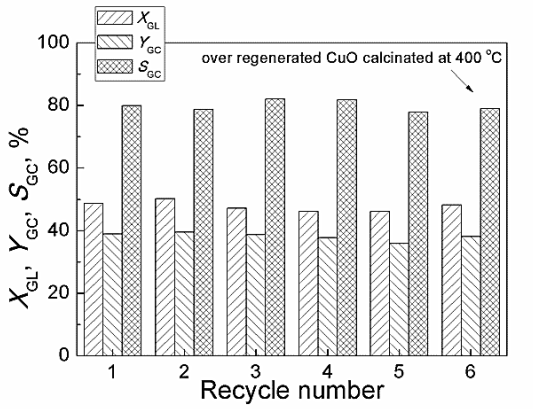

Figure 11: The stability of CuO-PT-400 nanoparticle catalyst on the reaction of GL with CO_2 (reaction condition: 40 mmol GL, 1.2 g Catalyst, 5 g of 2-Cyanopyridine, 15 g of DMF, 150°C, 4 MPa CO_2 and 5.0 h).

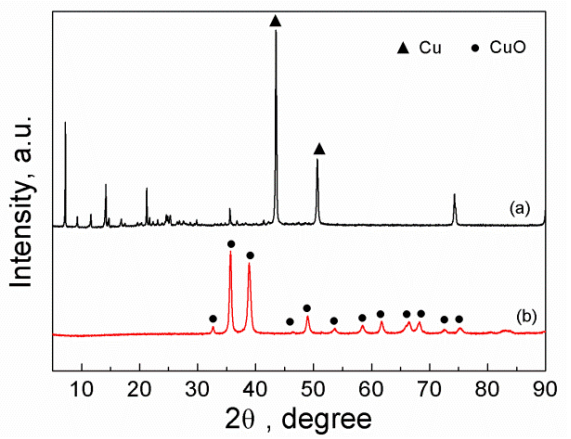

Figure 12: XRD patterns of the CuO nanoparticle catalysts: (a) the recovered CuO-PT-400 catalyst after the fifth recycling; (b) the recovered CuO-PT-400 catalyst again calcined at 400°C.

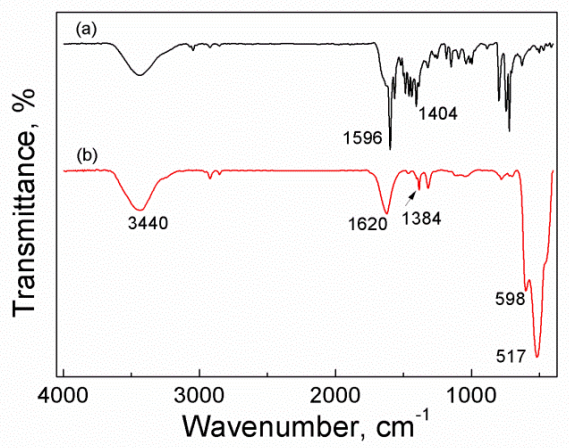

Figure 13: FT-IR spectra of CuO nanoparticles catalysts: (a) the recovered CuO-PT-400 catalyst after the fifth recycling; (b) the recovered CuO-PT-400 catalyst again calcined at 400°C.

can also reach 46.09% and 37.71%, respectively. At the fifth recycling, the GL conversion and GC yield reach 46.10% and 35.86%, respectively, indicating that the activity of CuO-PT-400 slightly decreases. In order to ascertain the reason of the decrease of the catalytic activity for the CuO-PT-400 catalyst, the recovered CuO-PT-400 in the fifth recycling was also characterized by XRD and FT-IR. Figure 12a shows that the crystalline structure of recovered CuO-PT-400 is changed, and it has a strong cubic Cu phase (2θ= 43.5°, 50.65°, see PDF 00-001-1242). Figure 13a shows that in the FT-IR spectra of recovered CuO-PT-400, the characteristic peaks attributed to Cu-O stretching mode (at 517 and 598 cm^{-1}) are vanished. These results imply that generation of Cu phase is responsible for the deactivation of the CuO-PT-400 catalyst. Interestingly, when the recovered CuO-PT-400 is calcined at 400°C, its main phase can be converted back into the monoclinic CuO again (Figures 12b and 13b). Meanwhile, the regenerated catalyst CuO-PT-400 was used to the reaction of GL and CO_2 and also can produce GL conversion of 48.25% and GC yield of 38.10% (Figure 11). It indicates that the recovered catalyst CuO-PT-400 can be easily regenerated by calcining at 400°C. Furthermore, the Cu concentration in the reaction mixture in the first run was also measured by ICP-MS and the result only was 45.12 μg/L indicate that the leaching of CuO almost can be neglected.

Conclusion

For the direct carbonylation of GL with CO_2 to produced GC, the efficient catalyst should have not only large amount of basic sites and surface area, but also high redox ability and oxygen vacancy. CuO nanoparticle calcinated at 400°C display high activity and stability and 2- cyanopyridine is the best dehydrating agent. The active site of CuO catalyst may be crystal face (111). Under condition of 150°C, 4 MPa, 5 h, the glycerol carbonate yield can reach about 40%.

The stability research for CuO nanoparticle shows that the catalyst can be reused five times with little loss of activity and can be easily regenerated by calcination at 400°C.

References

1. Okoye PU, Hameed BH (2016) Review on recent progress in catalytic carboxylation and acetylation of glycerol as a byproduct of biodiesel production. Renew Sust Energ Rev 53: 558-574.
2. Evangelista JPC, Gondim AD, Souza LD, Araujo AS (2016) Alumina-supported potassium compounds as heterogenerous catalysts for biodiesel production: A review. Renew Sust Energ Rev 59: 887-894.
3. Vyas AP, Subrahmanyam N, Patel PA (2009) Production of biodiesel through transesterification of Jatropha oil using KNO3/Al2O3 solid catalyst. Fuel 88: 625-628.
4. Baskar G, Aberna Ebenezer Selvakumari I, Aiswarya R (2018) Biodiesel production from castor oil using heterogeneous Ni doped ZnO nanocatalyst. Bioresour Technol 250: 793-798.
5. Moghzi F, Soleimannnejad J (2018) Sonochemical synthesis of a new nano-sized barium coordination polymer and its application as a heterogeneous catalyst towards sono-synthesis of biodiesel. Ultrason Sonochem 42: 193-200.
6. Ochoa-Gómez JR, Gómez-Jiménez-Aberasturi O, Maestro-Madurga B, Pesquera-Rodríguez A, Ramirez Lopez C, et al. (2009) Synthesis of glycerol carbonate from glycerol and dimethyl carbonate by transesterification: Catalyst screening and reaction optimization. Appl Catal A: Gen 366: 315-324.
7. Lu PF, Wang HJ, Hu KK (2013) Synthesis of glycerol carbonate from glycerol and dimethyl carbonate over the extruded CaO-based catalyst. Chem Eng J 228: 147-154.
8. Hu KK, Wang HJ, Liu YH, Liu Yang C (2015) KNO3/CaO as cost-effective heterogeneous catalyst for the synthesis of glycerol carbonate from glycerol and dimethyl carbonate. J Ind Eng Chem 28: 334-343.

9. Song XH, Wu YF, Cai FF, Pan DH, Xiao GM (2017) High-efficiency and low-cost Li/ZnO catalysts for synthesis of glycerol carbonate from glycerol transesterification: The role of Li and ZnO interaction. Appl Catal A: Gen 532: 77-85.

10. Okoye PU, Abdullah AZ, Hameed BH (2017) Stabilized ladle furnace steel slag for glycerol carbonate synthesis via glycerol transesterification reaction with dimethyl carbonate. Energy Conv Manag 133: 477-485.

11. Algoufi YT, Kabir G, Hameed BH (2017) Synthesis of glycerol carbonate from biodiesel by-product glycerol over calcined dolomite. J Taiwan Inst Chem Eng 70: 179-187.

12. Simanjuntak FSH, Widyaya VT, Kim CS, Ahn BS, Kim YJ, et al. (2013) Synthesis of glycerol carbonate from glycerol and dimethyl carbonate using magnesium-lanthanum mixed oxide catalyst. Chem Eng Sci 94: 265-270.

13. Lee Y, Lee JH, Yang HJ, Jang M, Kim JR, et al. (2017) Efficient simultaneous production of biodiesel and glycerol carbonate via statistical optimization. J Ind Eng Chem 51: 49-53.

14. Wu YF, Song XH, Cai FF, Xiao GM (2017) Synthesis of glycerol carbonate from glycerol and diethyl carbonate over Ce-NiO catalyst: The role of multiphase Ni. J Alloy Compd 720: 360-368.

15. Khanday WA, Okoye PU, Hameed BH (2017) Biodiesel byproduct glycerol upgrading to glycerol carbonate over lithium-oil palm ash zeolite. Energy Conv Manag 151: 472-480.

16. Alvarez MG, Frey AM, Bitter JH, Segarra AM, de Jong KP, et al. (2013) On the role of the activation procedure of supported hydrotalcites for base catalyzed reactions: Glycerol to glycerol carbonate and self-condensation of acetone. Appl Catal B Environ 134: 231-237.

17. Alvarez MG, Segarra AM, Contreras S, Sueiras JE, Medina F, et al. (2010) Enhanced use of renewable resources: Transesterification of glycerol catalyzed by hydrotalcite-like compounds. Chem Eng J 161: 340-345.

18. Rubio-Marcos F, Calvino-Casilda V, Banares MA, Fernandez JF (2010) Novel hierarchical Co3O4/ZnO mixtures by dry nanodispersion and their catalytic application in the carbonylation of glycerol. J Catal 275: 288-293.

19. Aresta M, Dibenedetto A, Nocito F, Ferragina C (2009) Valorization of bio-glycerol: New catalytic materials for the synthesis of glycerol carbonate via glycerolysis of urea. J Catal 268: 106-114.

20. Climent MJ, Corma A, Frutos PD, Iborra S, Noy M, et al. (2010) Chemicals from biomass: Synthesis of glycerol carbonate by transesterification and carbonylation with urea with hydrotalcite catalysts: The role of acid-base pairs. J Catal 269: 140-149.

21. Rahim MHA, He Q, Lopez-Sanchez JA, Hammond C, Dimitratos N, et al. (2012) Gold, palladium and gold-palladium supported nanoparticles for the synthesis of glycerol carbonate from glycerol and urea. Catal Sci Technol 2: 1914-1924.

22. Endah YK, Kim MS, Choi J, Jae J, Lee SD, et al. (2017) Consecutive carbonylation and decarboxylation of glycerol with urea for the synthesis of glycidol via glycerol carbonate. Catal Today pp: 293: 136-141.

23. Li HG, Xin CL, Jiao X, Zhao N, Xiao FK, et al. (2015) Direct carbonylation of glycerol with CO2 to glycerol carbonate over Zn/Al/La/X(X=F, Cl, Br) catalysts: The influence of the interlayer anion. J Mol Catal A Chem 402: 71-78.

24. Aresta M, Dibenedetto A, Nocito F, Pastore C (2006) A study on the carboxylation of glycerol to glycerol carbonate with carbon dioxide: The role of the catalyst, solvent and reaction conditions. J Mol Catal A-Chem 257: 149-153.

25. Liu JX, Li YM, Zhang J, He DH (2016) Glycerol carbonylkation with CO2 to glycerol carbonate over CeO2 catalyst and the influence of CeO2 preparation methods and reaction parameters. Appl Catal A: Gen 513: 9-18.

26. Zhang J, He DH (2014) Surface properties of Cu/La2O3 and its catalytic performance in the synthesis of glycerol carbonate and monoacetin from glycerol and carbon dioxide. J Colloid Interface Sci 419: 31-38.

27. Park CY, Nguyen-Phu H, Shin EW (2017) Glycerol carbonation with CO2 and La2O2CO3/ZnO catalysts prepared by two different methods: preferred reaction route depending on crystalline structure. Molecular Catalysis 435: 99-109.

28. George J, Patel Y, Pillai SM, Munshi P (2009) Methanol assisted selective formation of 1, 2-glycerol carbonate from glycerol and carbon dioxide using nBu2SnO as a catalyst. J Mol Catal A-Chem 304: 1-7.

29. Miwa T, Kaneco S, Katsumata H, Suzuki T, Onta K, et al. (2010) Photocatalytic hydrogen production from aqueous methanol solution with CuO/Al2O3/TiO2 nanocomposite. Int J Hydrog Energy 35: 6554-6560.

30. Bahmani M, Farahani BV, Sahebdelfar S (2016) Preparation of high performance nano-sized Cu/ZnO/Al2O3 methanol synthesis catalyst via aluminum hydrous oxide sol. Appl Catal A: Gen 520: 178-187.

31. Paulose S, Raghavan R, George BK (2017) Copper oxide alumina composite via template assisted sol-gel method for ammonium perchlorate decomposition. J Ind Eng Chem 53: 155-163.

32. Shokrani R, Haghighi M, Jodeiri N, Ajamein H, Abdollahifar M (2014) Fuel cell grade hydrogen production via methanol steam reforming over CuO/ZnO/Al2O3 nanocatalyst with various oxide ratios synthesized via urea-nitrates combustion method. Int J Hydrog Energy 39: 13141-13155.

33. Phiwdang K, Suphankij S, Mekprasart W, Pecharapa W (2013) Synthesis of CuO nanoparticles by precipitation method using different precursors. Energy Procedia 34: 740-745.